Astronomy
&
Astrophysics

Search for radiative pumping lines of OH masers

I. The 34.6 μm absorption line towards 1612 MHz OH maser sources[★,★★]

J. H. He[1], R. Szczerba[2], P. S. Chen[1], and A. M. Sobolev[3]

[1] National Astronomical Observatories/Yunnan Observatory, CAS, PO Box 110, Kunming, 650011, PR China
  e-mail: mailhejh@yahoo.com.cn
[2] N. Copernicus Astronomical Center, Rabiańska 8, 87-100 Toruń, Poland
[3] Astronomical Observatory, Ural State University, Lenin Street 51, Ekaterinburg 620083, Russia

Abstract. The 1612 MHz hydroxyl maser in circumstellar envelopes has long been thought to be pumped by 34.6 μm photons. Only recently, the Infrared Space Observatory has made possible spectroscopic observations which enable the direct confirmation of this pumping mechanism in a few cases. To look for the presence of this pumping line, we have searched the Infrared Space Observatory Data Archive and found 178 spectra with data around 34.6 μm for 87 galactic 1612 MHz masers. The analysis performed showed that the noise level and the spectral resolution of the spectra are the most important factors affecting the detection of the 34.6 μm absorption line. Only 5 objects from the sample (3 red supergiants and 2 galactic center sources) are found to show clear 34.6 μm absorption (all of them already known) while two additional objects only tentatively show this line. The 3 supergiants show similar pump rates and their masers might be purely radiatively pumped. The pump rates of OH masers in late type stars are found to be about 0.05, only 1/5 of the theoretical value of 0.25 derived by Elitzur (1992). We have also found 16 maser sources which, according to the analysis assuming Elitzur's pump rate, should show the 34.6 μm absorption line but do not. These non-detections can be tentatively explained by far-infrared photon pumping, clumpy nature of the OH masing region or a limb-filling emission effect in the OH shell.

Key words. masers – stars: AGB and post AGB – stars: circumstellar matter – radio lines: stars

1. Introduction

The first detection of intense radio emission from OH molecules was reported by Weaver et al. (1965) and soon an explanation based on maser amplification through induced processes was invoked (Litvak et al. 1966; Perkins et al. 1966). Shklovsky (1966) was the first to propose a radiative pumping mechanism for OH masers. Harvey et al. (1974) suggested that the correlation between the infrared (IR) and 1612 MHz variabilities observed in IR stars that exhibit this satellite line maser (hereafter OH/IR stars) is probably due to a radiative coupling mechanism between the stars and the OH clouds (radiative pumping of the maser, possibly at 2.8 μm or 34.6 μm). The idea of radiative pumping for OH/IR stars was then elaborated in detail by Elitzur et al. (1976),

who concluded that a pumping mechanism by far-infrared photons is more compatible with the observations. In this model, the required inversion of $F = 1$ and $F = 2$ sub-levels (even and odd parity, respectively) in the lowest rotational level of the OH molecule is achieved by absorption of infrared photons at 34.6 μm from the ground state ($^2\Pi_{3/2}\ J = 3/2$) and consequent radiative decays to lower levels via other far-infrared transitions. The final and the most crucial step in the pump cycle is the radiative decay from $^2\Pi_{1/2}\ J = 1/2$ to $^2\Pi_{3/2}\ J = 3/2$. If the transitions that link the two involved rotational level ladders are optically thick, a strong inversion of the level population that gives rise to the 1612 MHz maser can be produced. However, the fact that the 34.6 μm photons alone are enough to pump the 1612 MHz masers in OH/IR stars does not exclude that some other factors, such as collisional effects, line overlap, near infrared (NIR) pumping, might affect the maser pumping process. Elitzur et al. (1976) discussed these factors but did not include them in their model. Under the assumptions of optically thick far-infrared (FIR) pumping lines and saturated OH masers, their model showed that four FIR photons at 34.6 μm are needed to produce one maser photon at 1612 MHz. Bujarrabal et al. (1980) improved the OH 18 cm maser pumping model for circumstellar envelopes by adding

---

line overlap effects into the model. Their modeling work showed that FIR radiation together with the FIR line overlaps dominate the pumping of both OH main line and satellite line masers and the FIR line overlaps can strengthen the 1612 MHz maser. In order to explain the intensities of the main line OH masers observed in OH/IR stars and type II Miras, Collison & Nedoluha (1994) included additional processes in their OH maser model: non-local FIR line overlaps, collisional excitations, dust FIR pumping. They also investigated the importance of NIR line overlap and pointed out that the NIR line overlap between OH and H_2O can be important for the inversion of main line OH masers in thinner envelopes. Thai-Q-Tang et al. (1998) also developed an OH maser model to reproduce the observed FIR OH absorption lines in a red supergiant (RSG) OH maser: IRC+10420. Their model included collisional and FIR pumping but the line overlaps were only considered among the microwave transitions in the ground rotational level. They found that the observed maser properties are better reproduced if the Doppler shift is confined to a small range ($\sim$2 km s^{-1}), and argued that other processes such as a clumpy nature of the OH shell, NIR line overlaps or local thermal line overlaps may also play important roles in the pumping of the OH masers. Conclusively, we can say that problems related to the OH maser pumping are still poorly understood and therefore are worthy of further efforts. One of the main purposes of this paper is to search for more evidence of the FIR radiative pump mechanism in OH 1612 MHz maser sources.

Although the radiative pumping mechanism for the stellar 1612 MHz OH masers by the 34.6 μm line has been proposed long ago, its direct confirmation by observations became possible only after the launch of the Infrared Space Observatory (ISO, see Kessler et al. 1996). The 34.6 μm line was found in the red supergiant NML Cyg by Justtanont et al. (1996), and in the ISO spectrum obtained with the aperture centered on the galactic center object Sgr A* by Lutz et al. (1996). Then, Sylvester et al. (1997) found it together with the other OH rotational cascade emission lines at 79, 98.7 and 163 μm towards IRC+10420, another well known supergiant. The 1612 MHz OH maser in the envelope of this star was modeled by Thai-Q-Tang et al. (1998) who showed that these observations confirmed the radiative pumping of the maser by 34.6 μm line radiation. The 34.6 μm absorption feature was also reported by Neufeld et al. (1999) for another supergiant, VY CMa, and by Goicoechea & Cernicharo (2002) in the ISO spectra taken towards another galactic center object Sgr B2. Note that the 34.6 μm absorption feature has also been found in ISO spectra associated with four megamasers: the famous interacting galaxy Arp 220 (Skinner et al. 1997), the starburst galaxy NGC 253 (Bradford et al. 1999), IRAS 20100−4156 and probably III Zw 35 (Kegel et al. 1999). All these galaxies are predominantly 1667 MHz main line OH masers and in such cases the radiative pumping mechanism requires additional conditions to be fulfilled (see e.g. Elitzur 1978; Bujarrabal et al. 1980 or Elitzur 1992 for more detailed discussion). In this paper we concentrate on the galactic OH masers in the satellite line at 1612 MHz.

The discoveries mentioned above call for a more systematic check of the expected general presence of the 34.6 μm OH absorption line in other ISO spectra that are associated with the galactic OH-IR objects (i.e. OH/IR stars and non-stellar IR sources with OH masers). We have searched for the 34.6 μm feature in the ISO database for all 1612 MHz OH-IR objects irrespective of their evolutionary status (i.e. AGB stars, young stellar objects, molecular clouds, etc.) to check the frequency of the detection of this line. A preliminary analysis of available ISO data around 34.6 μm for OH-IR objects from the Chen et al. (2001) catalog has been presented by Szczerba et al. (2003). Here we present an improved analysis of 178 ISO Short Wavelength Spectrometer (SWS – de Graauw et al. 1996) spectra obtained towards 87 galactic OH-IR objects with the aim to search for the 34.6 μm OH absorption line. In Sect. 2 we describe our sample of galactic OH-IR objects and the data processing. The analysis of the detection rate of the 34.6 μm line is given in Sect. 3 and is followed by the discussion of pump rate for sources with detection and possible explanations for the absence of the pumping line in sources with non-detection of the 34.6 μm absorption line in Sect. 4. A summary is presented in Sect. 5. In future papers we will analyze the available ISO data to search for other OH rotational absorption and cascade emission lines.

2. Observations and data processing

The present version of Chen's catalog (unpublished) of 1612 MHz OH maser sources contains 1940 galactic objects. These OH sources were cross-correlated with the IRAS Point Source Catalog (PSC). Out of the 1940 entries, 1876 objects have their maser positions not farther than 1′ from the positions of the nearest IRAS PSC object and they constitute our working sample of galactic OH-IR objects in this paper[1]. Among them, 1070 OH-IR objects have IRAS Low Resolution Spectra (LRS) in the catalog of Kwok et al. (1997). Chen et al. (2001) have discussed the statistical properties of a somewhat smaller sample of 1024 galactic OH-IR objects with LRS spectra. Note that in that sample there was one object (IRAS 16527−4001) counted twice (sequential numbers 222 and 645 in their Table 1, with entry 645 being the correct one – the source belongs to the group A). Also, IRAS 16279−4757 with sequential number 778 and IRAS 19327+3024 with sequential number 865 in their paper, turned out to be absorption and non-detection at 1612 MHz, respectively. The total number of OH-IR sources in Chen et al. (2001) is actually 1021. The present sample of 1070 galactic OH-IR objects that have the IRAS association better than 1′ and have LRS spectra contains 49 new objects. All these 49 new maser sources are listed in Table 1a[2] which is an extension of

---

[1] Note again that an OH-IR object does not mean the OH/IR star defined by Habing (1996). The *OH-IR objects* considered here include not only evolved stars but also H II regions, young stellar objects and molecular clouds (see Col. (3) of Table 1b for details).

[2] The following papers have been cited in Table 1a: Chengalur et al. (1993), Eder et al. (1988), Lewis et al. (1990), Lewis (1992, 1994), Sevenster et al. (1997, 2001), Dickinson & Chaisson (1973), Szymczak et al. (2001), te Lintel Hekkert et al. (1989).

Table 1 of Chen et al. (2001) and has the same structure as their Table 1. That is to say, the sources in Table 1a are grouped using the University of Calgary LRS classification scheme with the letter codes defined by Volk & Cohen (1989) and, within each LRS group, ordered by right ascension. The last column of Table 1a contains information about references for the OH maser observations. Note that due to better maser position determination (ATCA3 - Sevenster et al. 2001), the 4 sources (IRAS 18440−0020, IRAS 18443−0147, IRAS 18102−1828, and IRAS 18449−0514), which were denoted by "1" in the Table 1 of Chen et al. (2001) (meaning that the radio and IRAS positions differ by more than 1′ and hence these objects were not counted as OH-IR sources), are now included in Table 1a as OH-IR objects.

We have searched the ISO Data Archive for SWS observations around 34.6 μm taken within 1′ of the IRAS position for all the 1876 OH-IR objects. There are 86 sources with a total of 170 SWS spectra that cover the wavelength region of interest. We also added NML Cyg to our sample. This object has no IRAS name, but it has 8 associated 34.6 μm ISO SWS spectra. Hence the total number of galactic OH-IR objects considered in this paper is 87 and the number of their ISO SWS spectra is 178.

The ISO Spectral Analysis Package (ISAP 2.1)[3] was used to process and analyze the 178 spectra in our sample. During data reduction, glitches were removed carefully, but small memory effects were smeared out by direct averaging across the two sub-scans. However, in the case of large memory effects, the up and down scans were averaged separately to verify the reality of the 34.6 μm absorption feature.

ISO spectra observed in different AOTs or speed modes have different spectral resolutions. Most of the OH-IR objects in the sample have only ISO SWS 01 spectra available. The ISO SWS 01 data were obtained in four speed modes: 1, 2, 3 or 4, with corresponding spectral resolution at 34.6 μm of about 400, 500, 800 and 1500, respectively. The remaining spectra in the sample were taken with ISO SWS 02, 06 or 07 modes for which the spectral resolutions are about 2250, 1500 and 30 000, respectively. Among the 178 analyzed ISO SWS spectra, 126 are SWS 01 (with 50 of them obtained in speed 1, 45 in speed 2, 22 in speed 3 and 9 in speed 4 mode), 23 are SWS 02, 20 are SWS 06 and 9 are SWS 07 spectra.

The details of our search and analysis are given in Table 1b[4] The OH-IR objects in Table 1b are grouped according to the detection of 34.6 μm absorption line and ordered within each group by their IRAS name while the spectra belonging to the

same OH-IR object are ordered by their TDT number. An object is classified as: group "A" if it has at least one "a"-type spectrum; group "T" if it has at least one "t"-type spectrum but no "a"-type spectrum; group "U" if it has only "n"-type and at least one "u"-type spectra; group "N" if it has only "n"-type spectra. Our definition of the ISO spectra is given below and described in more details in Sect. 3.1.

The above classification of the analysed objects is given in Col. (1) of Table 1b. The other columns contain the following data: (2) – the IRAS name; (3) – the class of the object as defined in SIMBAD (http://simbad.u-strasbg.fr/), and the abbreviations that are explained in the corresponding ReadMe file; (4) – the TDT number (Target Dedicated Time: the number that identifies an ISO observation); (5) – ISO Astronomical Observational Template (AOT), with number in parentheses showing the scan speed for SWS 01 spectra; (6) – a coding (Sp) related to the 34.6 μm line in the spectrum ("a": the absorption at 34.6 μm is detected; "t": it is tentatively detected; "u": it is undetected while we expect that it should be seen; and "n": the spectrum has too small resolution and/or is too noisy and/or the expected strength of the 34.6 μm line is too weak – the attribution of the code letter for each spectrum is explained in Sect. 3.1); (7) – the continuum flux around 34.6 μm ($F^{\rm c}_{34.6}$) for each spectrum; (8) – the 1σ noise level of the 34.6 μm spectrum, which is computed as the average of the standard deviations of all the data points in the range from 34.3 to 34.9 μm – the reciprocal of this quantity is proportional to the signal to noise ratio of the spectrum; (9) – the representative 34.6 μm continuum flux level for each OH-IR object ($\bar{F}^{\rm c}_{34.6}$) – it is derived by averaging mainly among good-quality SWS 01 spectra of each object; (10) – the line center flux density of the 34.6 μm feature with the continuum base subtracted ($F^{\rm p}_{34.6}$) (it is computed only for spectra that show this absorption line and a negative value means that the line feature is in absorption); (11) – notes related to $F^{\rm p}_{34.6}$; (12) – the blue peak flux density of the OH 1612 MHz maser emission ($F^{\rm p,blue}_{\rm OH}$); (13) and (14) – references and notes, respectively, for the maser peak fluxes with abbreviations explained at the end of the table. More detailed explanations for some of the quantities shown in Table 1b are given below.

3. The 34.6 μm absorption line

The detection rate of the 34.6 μm line can be affected by at least four factors: (1) spectrum resolution; (2) noise level; (3) continuum flux level around 34.6 μm; and (4) intrinsic line strength. The first two factors interplay with each other in determining the appearance of any line feature in the spectrum: for a lower resolution the absorption line is shallower and hence a lower noise level is required for the line to be resolved. The 34.6 μm feature is more easily detected when the adjacent continuum flux is high, since in this case, for a given observational set-up, the signal to noise ratio is higher. Finally, the intrinsic 34.6 μm line strength is a critical factor which can override all of the above factors: for a weaker line, a higher resolution and/or higher signal to noise ratio are required to detect the line. In the next sub-section, we introduce a quantitative concept of the 34.6 μm line detectability that takes into account all these

---

[3] The ISO Spectral Analysis Package (ISAP) is a joint development by the LWS and SWS Instrument Teams and Data Centers. Contributing institutes are CESR, IAS, IPAC, MPE, RAL and SRON.

[4] The following papers have been cited in Table 1b: Braz et al. (1990), Chengalur et al. (1993), David et al. (1993), Dickinson & Chaisson (1973), Eder et al. (1988), Engels (1979), Ivison et al. (1994), Le Squeren et al. (1992), Lewis (1994), Likkel (1989), Sevenster et al. (1997, 2001), Silva et al. (1993), Szymczak et al. (2001), te Lintel Hekkert (1990, 1991), te Lintel Hekkert & Chapman (1996), te Lintel Hekkert et al. (1989, 1991), Wilson & Barrett (1972), Zijlstra et al. (1989).
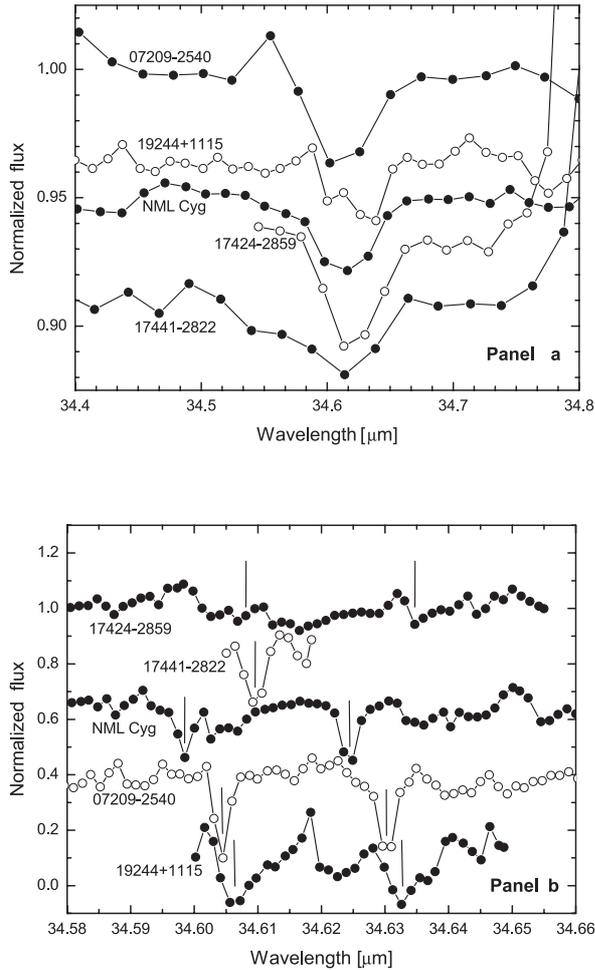
Fig. 1. The representative 34.6 μm absorption line profiles for the 5 detection objects. Panel **a)** shows the best spectra among the SWS 01, 02 or 06 ones of each object; panel **b)** shows the best SWS 07 spectrum of each object. The line centers or the expected line centers of the 34.6 μm doublet in panel **b)** are marked by short vertical lines. The spectra in both panels have been shifted arbitrarily for the sake of convenience. The TDT identification of the spectra shown in the figure are as follow: IRAS 07209−2540 (73402218, 73601963); IRAS 17424−2859 (09401504, 69602001); IRAS 17441−2822 (28702002, 46001217); IRAS 19244+1115 (36401631, 36401613); NML Cyg (52200719, 52200201).

factors, and we will discuss the effects of each of them on our spectra.

3.1. The 34.6 μm absorption line in the sample spectra

There are only 5 objects that show the 34.6 μm absorption line in the ISO SWS spectra (all of them have been discussed by other authors). In Fig. 1, representative spectra are shown for these 5 objects. Panel *a* of the figure shows the best spectra of SWS 01, 02 or 06 mode for each of them, while panel *b* shows their best SWS 07 spectra (resolution $R = 30\,000$). Note that variations of the wavelength positions of the 34.6 μm doublet, as clearly seen in panel *b* of the figure, are possibly due to the different radial velocities of these objects.

The remaining objects, except some tentative detections discussed below, do not show the 34.6 μm absorption line. In order to understand such a high number of non-detections, we start with an estimation of the expected strength of the 34.6 μm line for each spectrum, using available observational data. Theory predicts that about four 34.6 μm photons are needed to produce one 1612 MHz maser photon in a radiatively pumped maser (Elitzur 1992). This can be expressed as $N_{34.6}^{\text{int}} = 4\,N_{\text{OH}}^{\text{int}}$, here the left quantity is the integrated photon flux of the 34.6 μm absorption and the right quantity is the integrated photon flux of the 1612 MHz OH maser emission. Although some OH masers in our sample may not be radiatively pumped, we still can temporarily assume that they are all radiatively pumped so as to define a "pseudo" 34.6 μm absorption line strength from the maser strength for each of them. These "pseudo" line strengths should be quite different from their real 34.6 μm line strengths, and hence we may be able to use this difference as a diagnostic tool to identify them. For a line at a frequency ν, the integrated photon flux N^{int} is related to the integrated energy flux F^{int} by $N^{\text{int}} = F^{\text{int}}/h\nu$. The peak flux density of this line, F^{p}, is related to F^{int} by $F^{\text{int}} \approx F^{\text{p}}\Delta\nu = F^{\text{p}}\,\Delta V\,\nu/c$ (where $\Delta\nu$ is the line width in Hz, ΔV is the line width in velocity range and c is the speed of light). Assuming further that the maser emission and IR absorption occur in the same volume of gas, the velocity range (ΔV) of the maser line and of its pumping lines should be similar. Therefore, the OH-maser radiative pumping mechanism expressed by integrated photon fluxes above can be transformed into a relation between peak flux densities: $F_{34.6}^{\text{p}} = 4\,F_{\text{OH}}^{\text{p}}$. We consider only the blue peak fluxes ($F_{\text{OH}}^{\text{p,blue}}$) for double peaked OH 1612 MHz masers because the observed absorption at 34.6 μm is produced by the near side of the circumstellar envelope. For sources with a single peak maser, we take the only peak as the blue one (see the note mark "1p" in Col. (14) of Table 1b). The blue peak OH 1612 MHz maser emission flux densities are collected from the literature and presented in Col. (12) of Table 1b for each OH-IR object.

The measured depth of a line in a real spectrum also depends on the spectral resolution. It is clear that the more points we have within the line profile the better information we have about the line depth. There is no general agreement on how many points in a line profile are necessary to detect the line clearly. Our further considerations show that the assumption that at least 4 sampling points within the line profile are necessary to resolve the line clearly is appropriate for our study. In this case, with $\Delta V \approx V_{\text{exp}} \approx 20\,\text{km s}^{-1}$ for a typical circumstellar masing shell, a resolution of $R \approx 45\,000$ is required at 34.6 μm. Therefore, the expected peak flux density of the 34.6 μm line in a spectrum obtained with resolution R can be expressed as:

$$F_{34.6,\text{exp}}^{\text{p}} = 4\,F_{\text{OH}}^{\text{p,blue}}\,R/45\,000.$$

This formula is valid for almost all of our SWS spectra except the SWS 07 ones for which the 34.6 μm doublet is clearly resolved into two components. In this case, the above reasoning is only valid for the estimation of the depth of only one fine structure component and hence, assuming that the strengths of
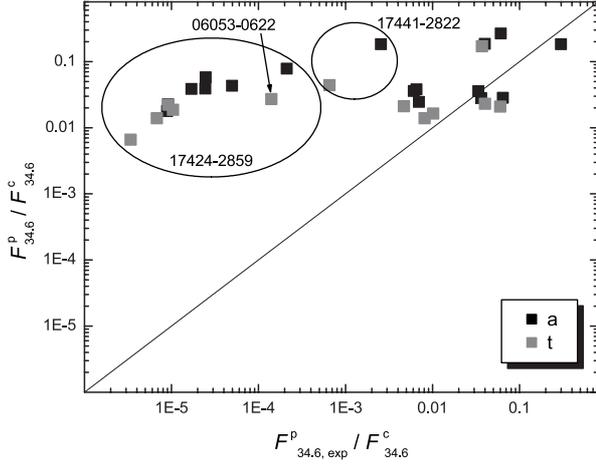
Fig. 2. The 34.6 μm absorption line depths measured in the spectra versus the expected values for these spectra (both divided by continuum flux $F^c_{34.6}$). The location of the spectra of IRAS 17424−2859, IRAS 17441−2822 and IRAS 06053−0622 are indicated explicitly. The adopted classification of the spectra (a, t) is explained in Sect. 3.1.

the two components are the same, the depth of a single component becomes:

$$F^p_{34.6,exp} = 2 F^{p,blue}_{OH} R/45\,000.$$

However, prominent uncertainties may exist in the two formulae. The line widths of the 34.6 μm absorption and the 1612 MHz OH maser emission peaks may actually be different and both of them may be smaller than the expansion velocity of the envelope ($\approx$20 km s^{-1}). These differences may cause changes in the coefficients of the two formulae. Thus it is necessary to verify the above formulae by comparing (in Fig. 2) the observed value $F^p_{34.6}$ (given in Col. (10) of Table 1b) with the relevant estimated value $F^p_{34.6,exp}$ for all the spectra in which the 34.6 μm absorption line has been clearly detected. In Fig. 2, both quantities have been divided by the corresponding 34.6 μm continuum flux level ($F^c_{34.6}$ given in Col. (7) of Table 1b) to remove the effect of different distances and different continuum flux levels. Excluding the spectra of IRAS 17424−2859, IRAS 17441−2822 and IRAS 06053−0622 (see discussion below), we conclude, by comparison with the one-to-one line, that the *expected* line depths agree in order of magnitude with the measured depths. This gives us confidence that the above two formulae and their coefficients are good enough to be used for the estimation of a reasonable *expected* 34.6 μm line strength. Comparison of the *expected* line strength with the noise level of the spectrum will allow us to determine whether the absence of the 34.6 μm absorption line in so many spectra is due to too high spectral noise.

Usually a line is considered as detected if its peak intensity is at least 3 times the root mean square noise level σ of the spectrum. In Fig. 3 we plot $F^p_{34.6,exp}/F^c_{34.6}$ as a function of $3\sigma/F^c_{34.6}$ for all the spectra of our sample. Squares (black and grey) correspond to objects for which the 34.6 μm absorption line depth has been derived. The solid line corresponds to $F^p_{34.6,exp} = 3\sigma$. As can be seen from the figure, we have been able to detect the 34.6 μm absorption line in some spectra with $F^p_{34.6,exp}$ significantly lower than 3σ (down to 3σ/10, as shown by the filled
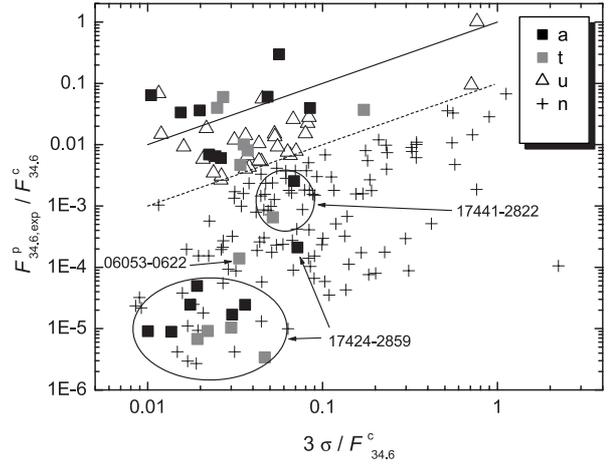

Fig. 3. The expected 34.6 μm absorption line depth estimated using OH 1612 MHz maser blue peak flux shown against the 3σ noise level (both divided by continuum flux $F^c_{34.6}$) for all the sample spectra. The solid and dotted lines mark where the expected 34.6 μm absorption line depth equals to the 3σ noise and tenth of the 3σ noise, respectively. The location of the "a" and "t" spectra of IRAS 17424−2859, IRAS 17441−2822 and IRAS 06053−0622 are indicated explicitly. The adopted classification of the spectra (a, t, u, n) is explained in Sect. 3.1.

or grey squares above the dotted line in the figure). That is to say, in some cases, with an assumed maser pumping efficiency of 0.25, the real 34.6 μm absorption is deeper than the depth required to produce the observed maser flux. There are various reasons for this. For example, IR and maser variability may cause large uncertainty in the *expected* 34.6 μm absorption depth; the assumption of the same line width ΔV for both IR and maser lines may be inaccurate, although not seriously wrong; real masers may transform IR photons into maser photons less effectively than assumed in the model of Elitzur (1992); some OH masers may be hidden behind OH molecular clouds that absorb 34.6 μm photons but do not mase. The distribution of data points in Fig. 3 shows that we can take 3σ/10 as a conservative limit for the detection of the 34.6 μm line.

The above considerations allow us to assign a class to each spectrum (given in Col. (6) of Table 1b). Spectra in which the 34.6 μm line is detected and measured are assigned class "a" if $F^p_{34.6} \geq 3\sigma$ (full squares in Fig. 3) or class "t" if $F^p_{34.6} < 3\sigma$ (gray squares in Fig. 3). Spectra in which the 34.6 μm is not detected are assigned class "u" if $F^p_{34.6,exp} \geq 3\sigma/10$ (open triangles in Fig. 3) or class "n" if $F^p_{34.6,exp} < 3\sigma/10$ ("+" symbols in Fig. 3). In other words, in spectra of class "n", we do not expect to detect the 34.6 μm absorption because of too low resolution or too high noise level or too low continuum flux or too weak *expected* 34.6 μm line strength, even if the relevant OH masers are radiatively pumped. In spectra of class "u", one can expect to see the absorption on the basis of the radiative maser-pumping model, but it is actually not seen (the possible reasons are discussed in Sect. 4.2). The fact that many "n"-type spectra are located far below the dotted line in Fig. 3 implies that the 34.6 μm feature is not detected in these objects most probably due to its intrinsic weakness (their *expected* line strengths are far smaller than the noise level of the spectra).

The data points corresponding to IRAS 17424−2859 and IRAS 17441−2822 and IRAS 06053−0622 are below this limit. In case of the two galactic center (GC) sources IRAS 17424−2859 and IRAS 17441−2822, it is likely that the observed strong features at 34.6 μm are the result of absorption by intervening foreground gas in the direction of GC (see e.g. Kaifu et al. 1972, Scoville 1972 or Karlsson et al. 2003). On the other hand, for the SWS observations of IRAS 17424−2859 and IRAS 17441−2822 we assigned the OH maser OH 359.946−0.048 and OH 0.667−0.035, respectively. In the so crowded region such association could be un-physical and, therefore, we are aware of the fact that the un-usual behavior of these sources could also be related to the complexity of the galactic center region. In consequences, the quantities derived for them are probably untrustworthy. The situation of IRAS 06053−0622, classified by SIMBAD as an ultra-compact H II region, is different. The 34.6 μm absorp-tion seems to be present only in one of its SWS 06 spectra (TDT 71101802 – see Table 1b). The feature is clearly present in *all* detectors in the up-scan spectra while the down-scans are relatively noisy and it is difficult to recognize this weak fea-ture in them. In addition, the 1612 MHz OH maser peak flux is given in te Lintel Hekkert's Ph.D. Thesis (1990) but not in any of the published papers, which may indicate that the maser flux is not very reliable. Therefore, the large difference between the estimated and the observed 34.6 μm line depth for this object may be due to the bad quality of the observational data.

3.2. Spectra statistics

For the convenience of the discussion, the 178 analyzed ISO SWS spectra can be split into 2 broad families: "at" that merges the class-"a" and class-"t" spectra, i.e., spectra with the 34.6 μm line at least tentatively detected, and "un" that merges class-"u" and class-"n" spectra, i.e., spectra with the 34.6 μm line not detected.

Figure 4 illustrates how the detection rate of the 34.6 μm line depends on the resolution. The hatched and grey areas in the stack columns represent the number of "at" and "un" spec-tra, respectively, and each column corresponds to a single reso-lution, except resolution 400 and 500 which are combined into a single column "400 & 500". As seen, most of the spectra are taken with low resolution and, in consequence, the detec-tion of a relatively narrow line feature, such as the 34.6 μm one, is difficult. The detection rate of the 34.6 μm feature is very small (about 2%) for the low resolution bins 400 & 500 and 800, and much larger for higher resolution bins (30−67%). We call this dependence the *resolution selection effect* on the detection rate of the 34.6 μm absorption line. Note that, even in the highest resolution bin, the detection rate is far from 100%. This strongly suggests that factors other than just the lack of sufficient resolution play a role in the fact that the line is not detected in many objects.

Figure 5 illustrates how the detection rate of the 34.6 μm line depends on the noise level. The hatched and grey areas in the stack columns now represent the number of "at" and "un" spectra, respectively, obtained in different intervals of $3\sigma/F^{\rm c}_{34.6}$.
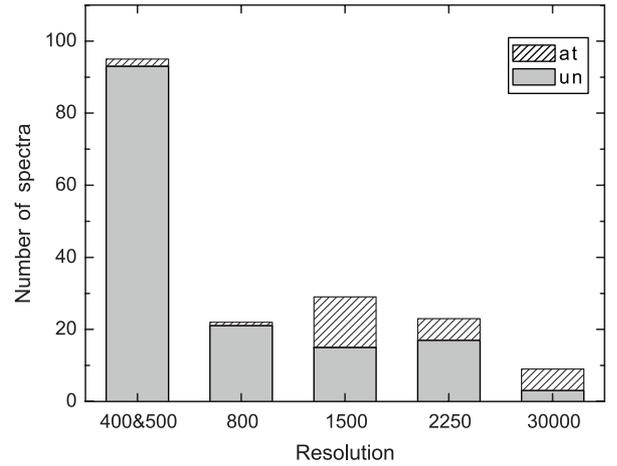

Fig. 4. Counts of ISO SWS spectra of different resolutions for galactic OH-IR objects. The two lowest resolutions are combined into a sin-gle column "400 & 500". The "at" and "un" type spectra are counted separately.
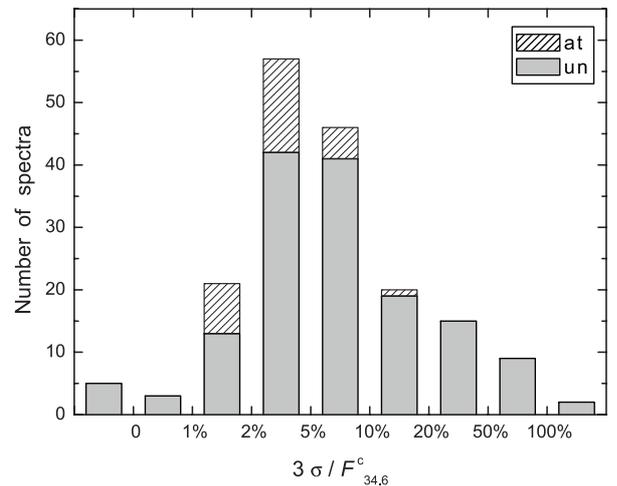

Fig. 5. Counts of ISO SWS spectra of different noise levels for galac-tic OH-IR objects. The negative flux level of the leftmost column is due to wrong dark subtraction from the spectra, the effect not cor-rected during our analysis. The "at" and "un" type spectra are counted separately.

It is seen that "at" spectra are found only for $3\sigma/F^{\rm c}_{34.6} < 20\%$. This is what we call the *sensitivity selection effect*. However, a significant fraction of non-detections occurs among spectra of intermediate signal-to-noise ratio and, most interestingly, the 34.6 μm line is not detected in any of the spectra with the high-est signal-to-noise ratio ($3\sigma/F^{\rm c}_{34.6} < 1\%$). This is due to the genuine weakness of the 34.6 μm line itself as can be inferred from Fig. 3.

Globally, the statistics of the detection of the 34.6 μm line in the 178 analyzed spectra is the following: there are 17 "a" spectra, 12 "t" spectra and 29 "u" spectra. Note that the majority of spectra (120) are of "n" type. Thus, ex-cluding the latter, we derive a meaningful detection-rate of (17+12)/(17+12+29) = 50%.
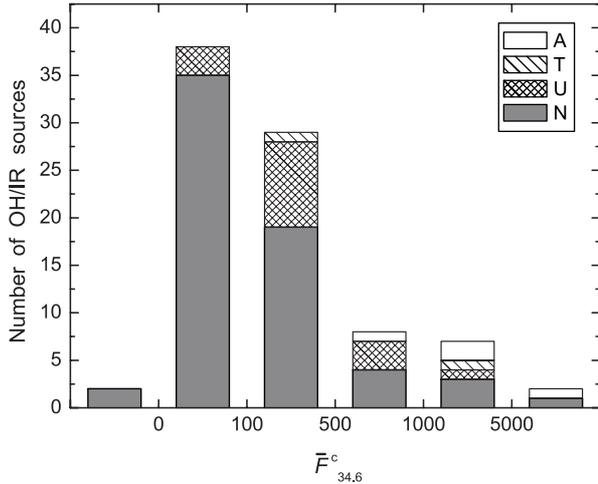
Fig. 6. Counts of sources in 5 intervals of the mean continuum flux around 34.6 μm. The leftmost bin corresponds to the sources which have only spectra with wrong dark current subtraction.

Fig. 7. The IRAS two color diagram for all our sample OH-IR objects with good quality fluxes at 12, 25 and 60 μm. The boxes marked on the plot are after van der Veen & Habing (1988).

3.3. Object statistics

We now turn to the discussion of objects statistics, grouping the sources as explained in Sect. 2. From Table 1b we see that only 5 galactic OH-IR objects definitely show the 34.6 μm absorption line ("A" sources). These are three red supergiants: NML Cyg, IRAS 19244+1115 = IRC+10420 and IRAS 07209−2540 = VY CMa and two sources related to the galactic center: IRAS 17424−2859 and IRAS 17441−28225. All of them were already known to have the 34.6 μm absorption feature. There are two more sources (IRAS 06053−0622 − an ultra-compact H II region and IRAS 17004−4119 – a Mira type) for which the 34.6 μm feature is tentatively detected ("T" sources).

In summary, out of 87 analyzed OH-IR objects, there are 5 with definite 34.6 μm detection, 2 with tentative detection, and 16 in which the detection of the 34.6 μm absorption should be possible according to our predictions, but actually was not. In all the remaining objects, the strength of the line estimated as explained in Sect. 3.1 is too low to allow detection in the analyzed spectra. Thus, the detection rate among objects with good enough spectra is (5+2)/(5+2+16) = 30%.

Of course, the detection rate might be biased by some observational effects linked to the properties of the source itself. The sample of sources we considered were chosen by different ISO observers for quite different observation purposes and is certainly not complete or uniform in any sense. For example, the incompleteness in the brightness distribution of the OH-IR objects can be a potential selection effect (*brightness selection effect*). And the infrared color distribution of the sample sources may be also incomplete (*color selection effect*).

Figure 6 illustrates how the detection rate of the 34.6 μm line depends on the continuum level. The white, hatched, crossed and grey surfaces in the stack columns represent the number of "A", "T", "U" and "N" sources in different intervals of $\bar{F}^c_{34.6}$ (from Col. (9) of Table 1b). Sources with wrong dark subtraction in their spectra are placed in the first bin ($\bar{F}^c_{34.6} < 0$). As already mentioned, $\bar{F}^c_{34.6}$ was obtained
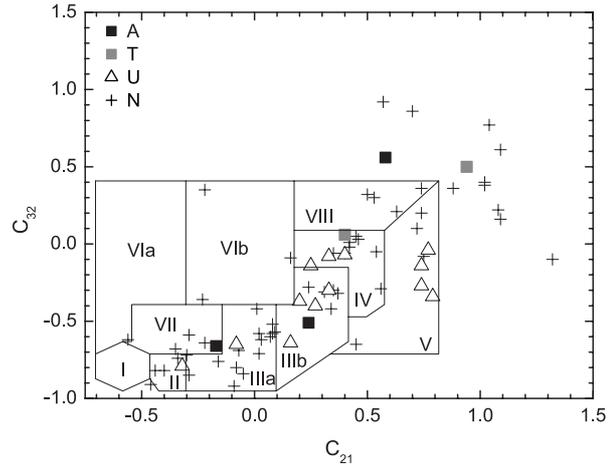
by averaging the 34.6 μm continuum fluxes of mainly the SWS 01 spectra. However, for some sources, SWS 01 data are not available and spectra obtained in other modes were used to estimate the continuum flux. They are: IRAS 03507+1115 (SWS 06 – TDT 80900805), IRAS 17441−2822 (SWS 07 – TDT 46001217), IARS 17462−2845 (SWS 02 – TDT 50601406) and IRAS 18349+1023 (SWS 02 – TDT 52302238). As Fig. 6 shows, the number of "A" or "T" sources increases from 0% for the first bin up to 50% for the bin representing the brightest sources, indicating the presence of a *brightness selection effect*. The fact that even among the brightest sources the detection rate is not 100% implies that this brightness selection effect cannot account for all cases in which the absorption at 34.6 μm is missing.

Now, let us investigate the position of our sources in the IRAS color-color diagram to check for a possible *color selection effect*. The $C_{32} = \log(F_{60}/F_{25})$ versus $C_{21} = \log(F_{25}/F_{12})$ color-color diagram for all OH-IR objects from our sample with good quality IRAS fluxes is shown in Fig. 7. For reference the regions defined by van der Veen & Habing (1988) are shown. As we can see, the sample sources are distributed in all areas where OH-IR objects may appear and there is no clear tendency of gathering for any type of sources. Therefore, we conclude that a *color selection effect* is not a severe problem in our sample.

4. The 1612 MHz OH maser pumping

4.1. The pump rate for type-A sources

For the five "A" type OH-IR objects, we can estimate a pump rate assuming that they are radiatively pumped. However, for the two GC sources, the physical association between IR sources and OH masers in the so crowded region as galactic center may be unphysical and, in addition, the observed 34.6 μm absorption may be due to absorption by intervening foreground gas (see discussion in Sect. 3.1). Therefore, we confine the discussion to the three supergiants.

Table 2. The 34.6 μm and 1612 MHz line parameters for the three supergiants which are used to estimate the OH maser radiative pump rate. The integrated fluxes $F_{34.6}^{\mathrm{int}}$ is in $[10^{-19}$ W/cm$^2]$, $F_{\mathrm{OH}}^{\mathrm{int,blue}}$ is in $[10^{-26}$ W/cm$^2]$ while the equivalent widths $EW_{34.6}$ is in $[10^{-4}\ \mu$m$]$. Negative values mean that the line is in absorption.

Name (1)	TDT[*] (2)	$F_{34.6}^{\mathrm{int}}$ (3)	$EW_{34.6}$ (4)	$F_{\mathrm{OH}}^{\mathrm{int,blue}}$ (5)	Pump rate (6)	References1 (7)	$F_{34.6}^{\mathrm{int,lit}}$ (8)	References2[**] (9)
IRAS 07209−2540	73103039	−18.7	−18.0	1751	0.052	tL-H(fig)[##]	−21.0	NEU99
	73402218	−21.4	−20.9					
	<u>73601963</u>	<u>−17.6</u>	<u>−16.2</u>					
IRAS 19244+1115	31600936	−4.12	−12.6	662	0.042	SYL97	−4.8	SYL97
	<u>36401613</u>	<u>−8.10</u>	<u>−21.0</u>					
	36401631	−3.31	−10.3					
	72400804	−6.49	−15.9					
NML Cyg	05200726	−34.7	−54.4	1154	0.052	priv(fig)[##]		
	34201475	−8.74[#]	−14.7[#]					
	<u>52200201</u>	<u>−11.5</u>	<u>−16.0</u>					
	52200719	−8.34	−16.8					
	52200720	−5.01	−9.34					
	53001311	−5.86	−11.0					
	74103105	−34.8	−49.3					

[*] The best spectrum together with its parameters are underlined for each source. They are used to estimate the pump rate.
[**] The reference codes in Col. (9): NEU99: Neufeld et al. (1999); SYL97: Sylvester et al. (1997).
[#] Only the sub-line No. 10 of 34201475 spectrum are used.
[##] (fig) means the integrated 1612 MHz OH maser fluxes are measured by us from the figure in the literature.

In Table 2 we list all the spectra (Col. (2)) with detected 34.6 μm line in the same order as in Table 1b. In Col. (3) we present the measured integrated flux of the 34.6 μm feature ($F_{34.6}^{\mathrm{int}}$) in 10^{-19} W/cm^2 ("-" sign means that the feature is in absorption), while in Col. (4) we give the equivalent widths ($EW_{34.6}$) in $10^{-4}\ \mu$m. These data are used in the comparison with the EWs of the 53.3 μm pumping line given in He & Chen (2004). For each source with multiple spectra, we choose the one with the highest spectral resolution (SWS 07) among the spectra of good quality. The best spectrum is underlined in Table 2 for each source and is used for the pump rate calculation below. Also included in Table 2 is the integrated blue peak flux of the OH 1612 MHz masers ($F_{\mathrm{OH}}^{\mathrm{int,blue}}$) in 10^{-26} W/cm^2 together with the corresponding references, in Cols. (5) and (7), respectively. The radiative pump rate defined as the ratio of integrated maser emission to integrated IR absorption ($F_{\mathrm{OH}}^{\mathrm{int,blue}} \nu_{34.6} / F_{34.6}^{\mathrm{int,best}} / \nu_{\mathrm{OH}}$) is presented in Col. (6). Column (8) gives the integrated line flux at 34.6 μm from the literature and Col. (9) shows the corresponding reference. Our line parameters are found to generally agree with those from the literature.

From Table 2, one can see that the pump rate is similar for all the three RSGs and is close to 0.05[5]. The similar pump

rates for the three RSGs may indicate that their OH 1612 MHz masers are radiatively pumped by the 34.6 μm line. A more complete discussion of the pumping mechanism in the case of RSGs is presented in He & Chen (2004), where the contribution of the 53.3 μm line is analysed.

If we adopt 0.05 as the pump rate of a typical radiatively pumped 1612 MHz OH maser, we will be in contradiction to the theoretic estimation that four 34.6 μm photons are needed to produce one 1612 MHz maser photon (a pump rate of 0.25). On the one hand, the too small pump rates (1/5 of the theoretic value 0.25) caution that Elitzur's model may be too simple to give a proper pump rate because many important processes (e.g. collisional effects, line overlap) are still absent in his model. On the other hand, the IR absorption line may be wider than the maser emission line and both lines may be narrower than the expansion velocity of the circumstellar envelope, and our assumptions (discussed in Sect. 3.1) can be responsible for a large difference between theoretical and the estimated pump rate. Note, however, that the two formulae used in this paper were more firmly justified by the one-to-one relation check shown in Fig. 2.

4.2. Why do we not see the 34.6 μm absorption in "U" type sources?

As we have discussed in Sect. 3.1, there are 16 OH-IR objects of which the *expected* 34.6 μm absorption line depth is large

[5] A formal estimation of the pump rate for the two GC sources (IRAS 17424−2859 and IRAS 17441−2822) gives very small values of $\approx$0.00007 (estimated from spectrum TDT 09500706: $F_{34.6}^{\mathrm{int}} = -27.7 \times 10^{-19}$ [W cm^{-2}] and data for OH 359.946−0.048: $F_{\mathrm{OH}}^{\mathrm{int,blue}} = 3.51 \times 10^{-26}$ [W cm^{-2}]), and $\approx$0.003 (estimated from spectrum TDT 46001217: $F_{34.6}^{\mathrm{int}} = -1.1 \times 10^{-19}$ [W cm^{-2}] and data for OH 0.667−0.035: $F_{\mathrm{OH}}^{\mathrm{int,blue}} = 6.0 \times 10^{-26}$ [W cm^{-2}]), respectively. On the other hand, it is worth to notice that the "pseudo" pump

rate for megamaser Arp 220 is close to 5! (estimated from spectrum TDT 11000803: $F_{34.6}^{\mathrm{int}} = -1.6 \times 10^{-19}$ [W cm^{-2}] and its single peak OH 1612 MHz data from Baan & Haschick (1987): $F_{\mathrm{OH}}^{\mathrm{int}} = 5700 \times 10^{-26}$ [W cm^{-2}]).

enough to be detected in at least some of their ISO SWS spectra but was not detected. In this section we discuss possible reasons for these non-detections.

The 34.6 μm photons are considered to be the main pumping mechanism for the OH 1612 MHz maser *only* in late type stars. The situation in other galactic sources (e.g. molecular clouds or H II regions) where the maximum of IR flux is shifted to much longer wavelengths is still far from being completely understood and it is quite possible that the OH maser pumping by longer wavelength IR photons (e.g. the 53.3 μm photons) could be dominant. The possibility of 1612 MHz OH maser pumping in these sources by the 53.3 μm photons is discussed in more detail in another paper (He & Chen 2004) devoted to the OH lines in the ISO Long Wavelength Spectrometer wavelength range.

Secondly, the non-detections could be related to the non-uniformity of the OH shell. Assuming that the 34.6 μm continuum emitting dusty medium is located mostly inside the OH maser shell, the absence of absorption at 34.6 μm may be explained by the clumpy nature of the OH shell. Dust grains effectively emitting 34.6 μm photons have a temperature above 100 K. For a typical circumstellar envelope of an AGB star, the dust temperature usually decreases from about 1000 K from the inner edge to about 100 K in the OH molecular shell. Hence the major parts of the 34.6 μm emitting region are located inside the OH shell and most of the 34.6 μm photons to pump the OH maser come from the hottest central region close to the central star. Therefore, it is possible that a sparsely distributed clumpy 1612 MHz OH maser shell obscures only a small part of the dust emitting region or even fails to cover the brightest central area of the IR emitting region. In such a situation, even if the number of 34.6 μm photons absorbed in the individual OH clumps is sufficient to pump the observed OH maser, the OH absorption efficiency integrated over the whole observable IR emitting area towards the observed source may be too small to produce an absorption line strong enough to be detected in the ISO SWS spectra. High spatial resolution interferometric observations (e.g. VLBI, MERLIN) of OH 1612 MHz masers show that the distribution of maser spots is not circular and sometimes delineates strip-like regions originating from the star (e.g. Richards et al. 1999; Zijlstra et al. 2001; Szymczak & Richards 2001; Gledhill et al. 2001; Bains et al. 2003). We are aware that due to strong beaming effects in maser amplification the apparent distribution of maser spots does not reflect the distribution of masing material adequately (see, e.g. Sobolev et al. 1998). However, the spread of maser spots delineates the region where significant absorption by the masing gas appears (Sobolev et al. 2004). Hence, interferometry of masers shows that the region masing at 1612 MHz does not encircle the whole IR emitting region of the star envelope. The spatial-velocity structure of OH maser clusters in OH/IR stars also shows that the distribution of the masing gas is likely to be non-spherically symmetric and traces the interface regions of the outflows that are known to be inhomogeneous (e.g., Zijlstra et al. 2001). Furthermore, high-resolution infrared imaging observations of dust emission from AGB or post-AGB stars also support the hypothesis of a clumpy nature of the circumstellar envelope (e.g., Goto et al. 2002; Monnier et al. 2004). Therefore, there are numerous pieces of evidence that the gas that mases at 1612 MHz does not form a complete IR screen surrounding the star. This makes the inhomogeneity of the OH "shell" a possible explanation for the large fraction of non-detections of the 34.6 μm OH absorption line.

Thirdly, it is possible that for relatively extended OH maser shells the limb-filling emission effect will play a role. A good example of this effect was demonstrated by modeling of the galactic center source Sgr B2 by Goicoechea & Cernicharo (2002). They set up a model by placing an infrared emitting sphere inside a surrounding OH shell. They found from their modeling that if the OH shell is too far away from the inner sphere that emits most of the infrared radiation or if OH shell itself is too geometrically thick, the observed OH infrared absorption lines will disappear due to the limb-filling emission effect. However, it is not obvious whether this model can be adopted for stellar OH-IR objects. On the other hand, if the OH shell is detached from the main body of the central infrared emitting region, the above scenario should be possible.

It is still tempting to consider collisional excitation of OH molecules as the main reason responsible for frequent non-detections of the 34.6 μm absorption line. However, collisional OH maser pumping has been considered as rather inefficient since the microwave OH maser and the infrared emission are observed to co-vary in most stellar OH-IR objects (Harvey et al. 1974). An additional argument against this mechanism (at least in the case of Sgr B2) comes from the ISO observations of OH Λ-doublets. These observations do not show any asymmetries in the line intensities of these infrared doublets while they are expected in the collisional pumping process (see Goicoechea & Cernicharo 2002 and references therein). One may argue that OH masers other than late type stars may exist in our sample of OH-IR objects and hence collisional pumping can be responsible for the missing of the 34.6 μm line in some sources. However, according to the SIMBAD classification, among the 16 type-U objects *only one* is classified as a molecular cloud while the other 15 are *stellar objects*. Therefore, it seems that collisional pumping cannot explain the non-detections discussed here.

The light variation in the IR and/or microwave ranges cannot be a major factor for the explanation of the non-detections. If sources are in minimum light during the ISO observation, their IR emission and hence radiative maser pumping process may be weaker, while on the other hand, if the relevant OH maser emission is in maximum light during the maser spectroscopic measurement (which is not simultaneous with the ISO measurement), the measured maximum maser flux will result in the estimation of a strong enough *expected* 34.6 μm absorption strength. In such a case, we are comparing a maximum *expected* 34.6 μm line strength with a minimum observed strength and non-detection (as for our type "U" sample sources) may occur. However this effect probably cannot explain all of our 16 type "U" sources because the IR light variations are usually small and it is unreasonable to assume that all of them were in minimum light at the time of the ISO observations and were in maximum light at the time of maser observations.

5. Summary

To search for the pumping line of the OH 1612 MHz masers we have analyzed 178 ISO SWS spectra taken around 34.6 μm for 87 OH-IR objects. The performed analysis shows that the 34.6 μm line is usually weak in our sample of OH-IR objects and the signal-to-noise ratio and spectral resolution of 120 spectra (among 178) are not high enough to resolve this feature. Among the 23 OH-IR objects associated with the remaining 58 spectra, 7 objects are of type "A" or "T" (the 34.6 μm line is detected or tentatively detected) and 16 objects are of type "U" (the 34.6 μm line is expected to be seen but it is not seen). Therefore, we obtain about 30% (7 out of 23) detections and about 70% (16 out of 23) non-detections. We have discussed some possible explanations for the 16 non-detections among the 23 OH-IR objects with reliable spectra, including FIR photon pumping, sparse distribution of the 1612 MHz maser spots and the limb-filling emission effect that could occur in a large OH shell.

The 34.6 μm absorption line is found only in three RSGs and two galactic center sources. The pump rates of red supergiants, calculated assuming that their 1612 MHz OH masers are radiatively pumped by this IR line, turned out to be similar and close to 0.05, a value which is only 1/5 of the theoretical value of 0.25. The similar pump rates of the 3 RSGs indicate that they might all be radiatively pumped.

References

Baan, W. A., & Haschick, A. D. 1987, ApJ, 318, 139 (BAA87)

Bains, I., Gledhill, T. M., Yates, J. A., & Richards, A. M. S. 2003, MNRAS, 338, 287

Bradford, C. M., Stacey, G. J., Fischer, J. A., et al. 1999, in The Universe as seen by ISO, ed. P. Cox, & M. F. Kessler, ESA SP-427, 861

Braz, M. A., Lépine, J. R. D., Sivagnanam, P., & Le Squeren, A. M. 1990, A&A, 236, 479 (BLS90)

Bujarrabal, V., Guibert, J., Nguyen-Q-Rieu, & Omont, A. 1980, A&A, 84, 311

Chen, P. S., Szczerba, R., Kwok, S., & Volk, K. 2001, A&A, 368, 1006

Chengalur, J. N., Lewis, B. M., Eder, J., & Terzian, Y. 1993, ApJS, 89, 189 (AOa)

Collison, A. J., & Nedoluha, G. E. 1994, ApJ, 422, 193

David, P., Le Squeren, A. M., & Sivagnanam, P. 1993, A&A, 277, 453 (DSS93)

de Graauw, T., Haser, L. N., Beintema, D. A., et al. 1996, A&A, 315, L49

Dickinson, D. F., & Chaisson, E. J. 1973, ApJ, 181, L135 (DC73)

Eder, J., Lewis, B. M., & Terzian, Y. 1988, ApJS, 66, 183 (AOb)

Engels, D. 1979, A&AS, 36, 337 (EN79)

Elitzur, M. 1978, A&A, 62, 305

Elitzur, M. 1992, Astronomical Masers (Kluwer Academic Publishers)

Elitzur, M., Goldreich, P., & Scoville, N. 1976, ApJ, 205, 384

Gledhill, T. M., Yates, J. A., & Richards, A. M. S. 2001, MNRAS, 328, 301

Goicoechea, J. R., & Cernicharo, J. 2002, ApJ, 576, L77

Goto, M., Kobayashi, N., Terada, H., & Tokunaga, A. T. 2002, ApJ, 572, 276

Habing, H. J. 1996, ARA&A, 7, 97

Harvey, P. M., Bechis, K. P., Wilson, W. J., & Ball, J. A. 1974, ApJS, 27, 331

He, J. H., & Chen, P. S. 2004, New Astron., 9, 545

Ivison, R. J., Seaquist, E. R., & Hall, P. J. 1994, MNRAS, 269, 218 (ISH94)

Justtanont, K., de Jong, Th., Helmich, F. P., et al. 1996, A&A, 315, L217

Kaifu, N., Kato, T, & Iguchi, T. 1972, PASJ, 26, 117

Karlsson, R., Sjouwerman, L. O., Sandqvist, A., & Whiteoak, J. B. 2003, A&A, 403, 1011

Kegel, W. H., Hertenstein, T., & Quirrenbach, A. 1999, A&A, 351, 472

Kessler, M. F., Steinz, J. A., Anderegg, M. E., et al. 1996, A&A, 315, L27

Kwok, S., Volk, K., & Bidelman, W. P. 1997, ApJS, 112, 557

Le Squeren, A. M., Sivagnanam, P., Dennefeld, M., et al. 1992, A&A, 254, 133 (SSD92)

Lewis, B. M. 1992, ApJ, 396, 251 (AO)

Lewis, B. M. 1994, ApJS, 93, 549 (AOe)

Lewis, B. M., Eder, J., & Terzian, Y. 1990, ApJ, 362, 634 (AO)

Likkel, L. 1989, ApJ, 344, 350 (L89)

Litvak, M. M., Mc Whorter, A. L., Meeks, M. L., & Zeiger, H. J. 1966, Phys. Rev. Lett., 17, 821

Lutz, D., Feuchtgruber, H., Genzel, R., et al. 1996, A&A, 315, L269 (LUT96)

Monnier, J. D., Millan-Gabet, R., Tuthill, P. G., et al. 2004, ApJ, 605, 436

Neufeld, D. A., Feuchtgruber, H., Harwit, M., & Melnick, G. J. 1999, ApJ, 517, L47 (NEU99)

Perkins, F., Gold, T., & Salpeter, E. E. 1966, ApJ, 145, 361

Richards, A. M. S., Yates, J. A., & Cohen, R. J. 1999, MNRAS, 306, 954

Scoville, N. Z. 1972, ApJ, 175, L127

Shklovsky, I. S. 1966, Astron. Tsirk., No. 372

Sevenster, M. N., Chapman, J. M., Habing, H. J., Killeen, N. E. B., & Lindqvist, M. 1997, A&AS, 122, 79 (ATCA)

Sevenster, M. N., van Langevelde, H. J., Moody, R. A., et al. 2001, A&A, 366, 481 (ATCA3)

Silva, A. M., Azcárate, I. N., Pöppel, W. G. L., & Likkel, L. 1993, A&A, 275, 510 (SAP93)

Skinner, C. J., Smith, H. A., Sturm, E., et al. 1997, Nature, 386, 472 (SKI97)

Sobolev, A. M., Wallin, B. K., & Watson, W. D. 1998, ApJ, 498, 763

Sobolev, A. M., Sutton, E. C., Cragg, D. M., & Godfrey, P. D. 2004, Ap&SS, in press [arXiv:astro-ph/0405286]

Sylvester, R. J., Barlow, M. J., Nguyen-Q-Rieu, et al. 1997, MNRAS, 291, L42 (SYL97)

Szczerba, R., He, J. H., & Chen, P. S. 2003, in Exploiting the ISO Data Archive – Infrared Astronomy in the Internet Age, ed. C. Gry, S. B. Peschke, J. Matagne, et al., ESA SP-511, 101

Szymczak, M., & Richards, A. M. S. 2001, in Post-AGB objects as a phase of stellar evolution, ed. R. Szczerba, & S. K. Górny (Kluwer Academic Publisher), ASSL, 265, 429

Szymczak, M., Szczerba, R., & Chen, P. S. 2001a, in Post-AGB objects as a phase of stellar evolution, ed. R. Szczerba, & S. K. Górny (Kluwer Academic Publisher), ASSL, 265, 439 (SSC01)

Thai-Q-Tang, Dinh-V-Trung, Nguyen-Q-Rieu, et al. 1998, A&A, 331, 317

te Lintel Hekkert, P. 1990, Ph.D. Thesis, University of Leiden (tL-HPhD)

te Lintel Hekkert, P. 1991, A&A, 248, 209 (tLH91)

te Lintel Hekkert, P., Caswell, J. L., Habing, H. J., et al. 1991, A&AS, 90, 327 (tL-H)

te Lintel Hekkert, P., & Chapman, J. M. 1996, A&AS, 119, 459 (LC96)

te Lintel Hekkert, P., Versteege-Hensel, H. A., Habing, H. J., & Wiertz, M. 1989, A&AS, 78, 399 (tLVHW)

van der Veen, W. E. C. J., & Habing, H. J. 1988, A&A, 194, 125

Volk, K., & Cohen, M. 1989, AJ, 98, 931

Weaver, H., Williams, D. R. W., Dieter, N. H., & Lum, W. T. 1965, Nature, 208, 29

Wilson, W. J., & Barrett, A. H. 1972, A&A, 17, 185 (WB72)

Zijlstra, A. A., te Lintel Hekkert, P., Pottasch, S. R., et al. 1989, A&A, 217, 157 (ZLP89)

Zijlstra, A. A., Chapman, J. M., te Lintel Hekkert, P., et al. 2001, MNRAS, 322, 280